NANO LETTERS

2009
Vol. 9, No. 7
2756-2762

Integrating Structure Control over Multiple Length Scales in Porous High Temperature Ceramics with Functional Platinum Nanoparticles

Marleen Kamperman,[†] Andrew Burns,[†] Robert Weissgraeber,[†] Niels van Vegten,[‡] Scott C. Warren,[†] Sol M. Gruner,[§,||] Alfons Baiker,[‡] and Ulrich Wiesner*[,†]

Department of Materials Science and Engineering, Department of Physics, Cornell High Energy Synchrotron Source (CHESS), Cornell University, Ithaca, New York 14853, and Department of Chemistry and Applied Biosciences, ETH Zürich, Hönggerberg − HCI, CH-8093, Zürich, Switzerland

Received April 23, 2009; Revised Manuscript Received May 29, 2009

ABSTRACT

High temperature ceramics with porosity on multiple length scales offer great promise in high temperature catalytic applications for their high surface area and low flow resistance in combination with thermal and chemical stability. We have developed a bottom-up approach to functional, porous, high-temperature ceramics structured on eight distinct length scales integrating functional Pt nanoparticles from the near-atomic to the macroscopic level. Structuring is achieved through a combination of micromolding and multicomponent colloidal self-assembly. The resulting template is filled with a solution containing a solvent, a block copolymer, a ceramic precursor, and a nanoparticle catalyst precursor as well as a radical initiator. Heat treatment results in three-dimensionally interconnected, high-temperature ceramic materials functionalized with well-dispersed 1−2 nm Pt catalyst nanoparticles and very high porosity.

Nature exhibits phenomenal diversity and control in the structural design of materials from cellulose aggregates in wood to silica nanostructures in diatom shells. These materials often integrate function through structural variations from the atomic scale all the way to the macroscale, tailored to create combinations of properties that are well-adapted to their purposes.[1] Fundamental understanding of a natural system challenges our ability to mimic Nature with the guiding philosophy that the only way to understand how to build a house is to build one yourself. Despite considerable progress in the field of nanotechnology, integration of function from the atomic or near-atomic scale to the macroscopic scale remains a major challenge. Here we demonstrate a synthetic high-temperature functional ceramic material prepared by soft matter assembly combining properties from eight components within a single highly porous material. We focus on functional Pt nanoparticles because it is widely recognized that hierarchically ordered pore structures in stable and robust catalyst supports are highly desirable. Macropores reduce flow resistance, allowing easy entry to the bulk of the material, where the large surface area of the mesopores can be effectively accessed.

A pioneering example (albeit without integrated function) of synthetically produced, porous oxide materials hierarchically ordered over multiple discrete length scales was based on the coassembly of triblock copolymers and sol−gel species with colloidal crystallization and micromolding.[2,3] Subsequent approaches for producing hierarchically ordered materials included microporous zeolitic colloids used as building blocks within a macrotemplate,[4,5] combinations of polystyrene (PS) spheres, block copolymer and "ionic liquid" templating,[6] multicomponent colloidal assembly[7,8] and hierarchically ordered carbon.[9,10] Unfortunately, the relatively low hydrothermal stability of mesoporous silica[11] and the combustibility of carbon in air at 500 °C[12] make these materials unsuitable for use in high temperature catalysis.

In contrast to oxide- and carbon-based porous materials structure directed by organic molecules, much less research has been conducted on porous nonoxide type ceramics derived from self-assembled composites. As a result of their excellent thermal and chemical stability, nonoxide materials such as silicon carbonitride are promising candidates as supports for high temperature catalysts. To this end, ordered and nonordered porous SiC and SiC_xN_y materials have been

* To whom correspondence should be addressed. Email: ubw1@cornell.edu.
[†] Department of Materials Science and Engineering, Cornell University.
[‡] ETH Zürich.
[§] Department of Physics, Cornell University.
[||] Cornell High Energy Synchrotron Source (CHESS), Cornell University.

10.1021/nl901293p CCC: $40.75
Published on Web 06/11/2009

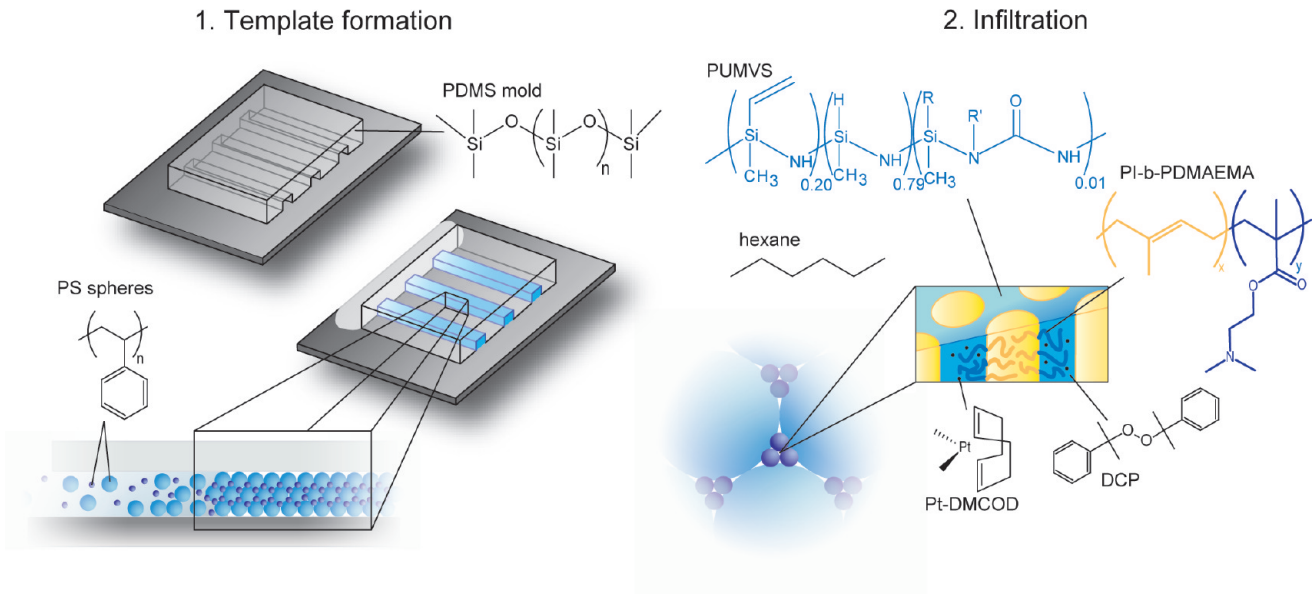

Figure 1. Schematic representation of the two step synthetic procedure. (1) Colloidal self-assembly of polystyrene spheres of two different diameters in the microchannels of a PDMS mold. (2) Infiltration of the packed three-component bed with the five-component precursor solution, consisting of amphiphilic block copolymer PI-*b*-PDMAEMA (PI is yellow and PDMAEMA is blue), ceramic precursor for SiCN type materials (PUMVS molecule has cyclic and linear features; R = H or vinyl, no information is available about the nature of R′), Pt nanoparticle precursor (Pt-DMCOD) and radical initiator all in hexane as solvent. Coassembly leads to nanostructured morphologies that can be permanently set by cross-linking the PUMVS. Temperature treatment up to 1000 °C results in a three-dimensionally interconnected, high-temperature ceramic material structure directed on eight different length scales that is functionalized with well-dispersed platinum nanoparticles.

developed.[13−15] Impregnation of a macroporous SiC with a ruthenium salt resulted in a catalyst with high conversions for the decomposition of ammonia at temperatures above 700 °C, which make these structures interesting candidates for hydrogen production.[16] Functional integration in this case, however, was limited to two length scales and required multiple synthetic steps.

Here we present highly porous high-temperature ceramic materials that are structured over eight discrete length scales and integrate Pt nanoparticles with catalytic functionality. We combined micromolding and two-component colloidal self-assembly with cooperative assembly of a five component precursor system (solvent, amphiphilic block copolymer, radical initiator, ceramic and platinum catalyst precursors) to obtain the desired materials. Heat treatment to 1000 °C led to three-dimensionally interconnected, hierarchically ordered, highly porous, high temperature ceramic materials functionalized with well-dispersed Pt nanoparticles. The level of structure control achieved here was enabled by considerable progress in the fields of porous high temperature SiCN-type ceramics from so-called polymer derived ceramic (PDC) precursors, micromolding and binary colloidal self-assembly over the last couple of years.[13,17−19] Experimental challenges that needed to be overcome included finding the right combination of colloidal particle sizes for the two-component colloidal crystal formation within the channels, selecting the right solvent providing high enough solubility for all solution components but without dissolving the colloidal template, and optimizing the solution viscosity for the precursor infiltration process into the colloidal template.

Figure 1 shows a schematic illustration of the two-step process used to obtain the integrated materials. The first step involved the colloidal self-assembly of PS spheres of two sizes in microchannels defined by a poly(dimethylsiloxane) (PDMS) mold. The mold provided 500 μm wide channels open at both ends with walls that integrated 60 μm wide channels. The mold was placed on a freshly cleaned Si wafer and a drop of PS sphere suspension in water was placed on one side of the mold. PS sphere sizes tested included combinations of 16.0, 3.0, 2.0, and 1.0 μm diameter spheres with 1.0 μm, 600, 350, 200, and 100 nm sized beads. The concentration ratios C_{small}/C_{large} were varied between 0.017 and 0.17. Best results were obtained with suspensions containing PS spheres with diameters of 3.0 μm and 350 nm in a concentration ratio of $C_{350nm}/C_{3\mu m} = 0.08$. Capillary action filled the channels with the colloidal suspension. Solvent evaporation from the open end of the channels acted as the driving force for sphere packing as the drying front progressed toward the reservoir side. The order and the type of binary lattice formed depended on the size, the size ratio, and relative concentrations of the spheres and could be altered to control the density of the final materials.[7,18,20−22]

The second step in the process was the infiltration of the packed three component bed with the five component precursor solution, consisting of a solvent, an amphiphilic block copolymer, a ceramic precursor for SiCN-type materials, a platinum nanoparticle precursor and a radical initiator. The challenge was to select the right solvent to ensure solubility of all components, even at high concentration (at the drying front), without dissolving the colloidal template. Initial experiments were pursued with tetrahydrofuran (THF) or toluene and cross-linked PS spheres. While these are excellent solvents for many organic materials, they led to significant deformations of colloid shape. After trying many

combinations of solvents and precursors, we arrived at the following materials and solvent choices. The block copolymer poly(isoprene-*block*-dimethylaminoethyl methacrylate) (PI-*b*-PDMAEMA) was used as a structure directing agent for the polymeric ceramic precursor, poly(ureamethylvinyl)-silazane (PUMVS) (see Figure 1 for molecular structures).[23] PUMVS is a PDC precursor, which starts out as a polymer that can be shaped into complex structures and solidified by cross-linking through polymerization with dicumyl peroxide as radical initiator. Heat treatment transforms the polymeric precursor into ceramic SiCN-type materials, while retaining the original (complex) shape as shown in multiple thorough investigations of bulk and mesoporous materials in the past.[24−27] Mixing PUMVS with this block copolymer was expected to lead to preferential swelling of the hydrophilic PDMAEMA domains with PUMVS due to its polar nature.[13] To generate an inverse hexagonal morphology with PI cylinders in a PUMVS/PDMAEMA matrix, a PI-*b*-PDMAEMA block copolymer with a total molecular weight of 31 kg/mol and 33 wt % PDMAEMA was mixed with PUMVS in a 1:2 ratio in hexane.[27] Dicumyl peroxide and dimethyl (1,5-cyclooctadiene) platinum (Pt-DMCOD) were added to the solution as radical initiator (to cross-link the PUMVS) and Pt nanoparticle precursor, respectively. Platinum was expected to preferentially segregate in the PDMAEMA domains, as the allyl groups of the PUMVS can efficiently add to Pt,[28] in a similar fashion to the double bond coordination of Pt with cyclooctadiene in the precursor molecule (see Figure 1 for the molecular structures of the ceramic and metal nanoparticle precursors).[29] A drop of this solution was placed on one side of the mold leading to interstitial space filling between the PS spheres by capillary action.

Another experimental challenge was optimizing the precursor solution viscosity. The viscosity had to be low enough to maintain porosity on all levels at the interface between the PDMS mold and the colloidal crystal, preventing a "closed" interface limiting the accessibility of the inner pores inside the channels in the final material. On the other hand, the viscosity had to be high enough to prevent lifting off of the mold from the Si substrate, in which case the integrity of the channel structure would have been lost. The largest contribution to solution viscosity arises from the polymers. Fixing the block copolymer:PUMVS ratio at 1:2, we varied the polymer (PI-*b*-PDMAEMA + PUMVS):hexane weight ratio between 0.15:1 and 0.60:1. Best results were obtained for a weight ratio of 0.5:1. The structure was permanently set by radically initiated cross-linking of the PUMVS at 130 °C. Careful removal of the mold and subsequent heat treatment under reducing atmosphere to 1000 °C simultaneously removed organic volatiles, converted the PUMVS into a ceramic, and reduced the Pt-precursor to its metallic form.

The final material shows ordering on eight distinct length scales as summarized in Figure 2. The upper part of Figure 2 a−i shows experimental imaging results while the lower part (j−q) depicts the eight structural levels in an illustration. On the macroscopic scale (5 mm) the shape of the sample is governed by the shape and size of the mold (Figure 2a,j). The ability to mold porous materials into any desired shape and size increases the range of applications significantly compared to a powder. The second and third levels of ordering (500 and 60 μm) are the microchannel patterns created by the micromold (Figure 2k,l). Figure 2b shows a light microscope image and Figure 2c,d show scanning electron microscopy (SEM) images of the heat treated material, demonstrating the quality of the channel reproduction. The fourth and fifth structural levels of ordering are controlled through colloidal crystal templating by two sizes of polystyrene particles (Figure 2e,f,m,n). The 3.0 μm latex spheres self-assembled into a close-packed lattice and the smaller 350 nm latex spheres were forced to pack into the interstices between the large micrometer-spheres. The close-packed arrangement of the PS spheres (touching spheres) resulted in interconnecting, uniform-sized windows, giving rise to additional pore sizes, as can be clearly seen in Figure 2e,f.

The sixth structure level is determined by the mesopores of the framework itself due to the microphase separation of the coassembled block copolymer and PUMVS into an inverse hexagonal pore structure (see SEM image in Figure 2f and transmission electron microscopy (TEM) image in Figure 2g as well as illustration 2o). The characteristic pore-to-pore distance was approximately 25 nm as estimated from TEM and SEM. The mesoporous nature of the pyrolyzed materials was confirmed by nitrogen physisorption (see Figure 3a). The material exhibits a type IV nitrogen sorption isotherm with specific surface area of 44 m^2/g. Barrett−Joyner−Halenda (BJH) pore size distribution, as derived from the nitrogen adsorption isotherm, reveals a uniform peak mesopore diameter of 11.0 nm,[30] in agreement with pore size estimates from SEM and TEM images (see Figure 2f−h, respectively). Small angle X-ray scattering (SAXS) confirms mesoporous ordering (see Figure 3b,A). The first order peak ($q^* = 3.15 \times 10^{-2}$ Å^{-1}) corresponds to a repeat spacing of 19.9 nm while the second and third order peaks at $3^{1/2}$ and $7^{1/2}$ times q^* are consistent with a hexagonal lattice. The lattice parameter corresponds to a pore-to-pore distance of 23.0 nm in good agreement with both SEM and TEM data.

The material shrank during heat treatment, resulting in a decrease in channel width (measured at the top surface) of 7−11% and a decrease in pore size from the colloidal crystal templating of 10−17% compared to the original PS sphere sizes, as determined from SEM images. The hexagonal lattice spacing decreased by 30% compared to as-synthesized bulk PI-*b*-PDMAEMA/PUMVS hybrid materials. The lattice spacings were not directly compared to infiltrated packed bed samples as the diffuse scattering of the PS spheres made quantitative spectral analysis difficult. The difference in shrinkage on the different length scales may in part be due to anisotropic behavior induced by the strong anchoring of the structure onto the Si substrate. This is suggested by earlier analysis of block copolymer-inorganic hybrid films subjected to heat treatments, showing uniaxial shrinkage as high as 30% along an axis perpendicular to the substrate surface.[31]

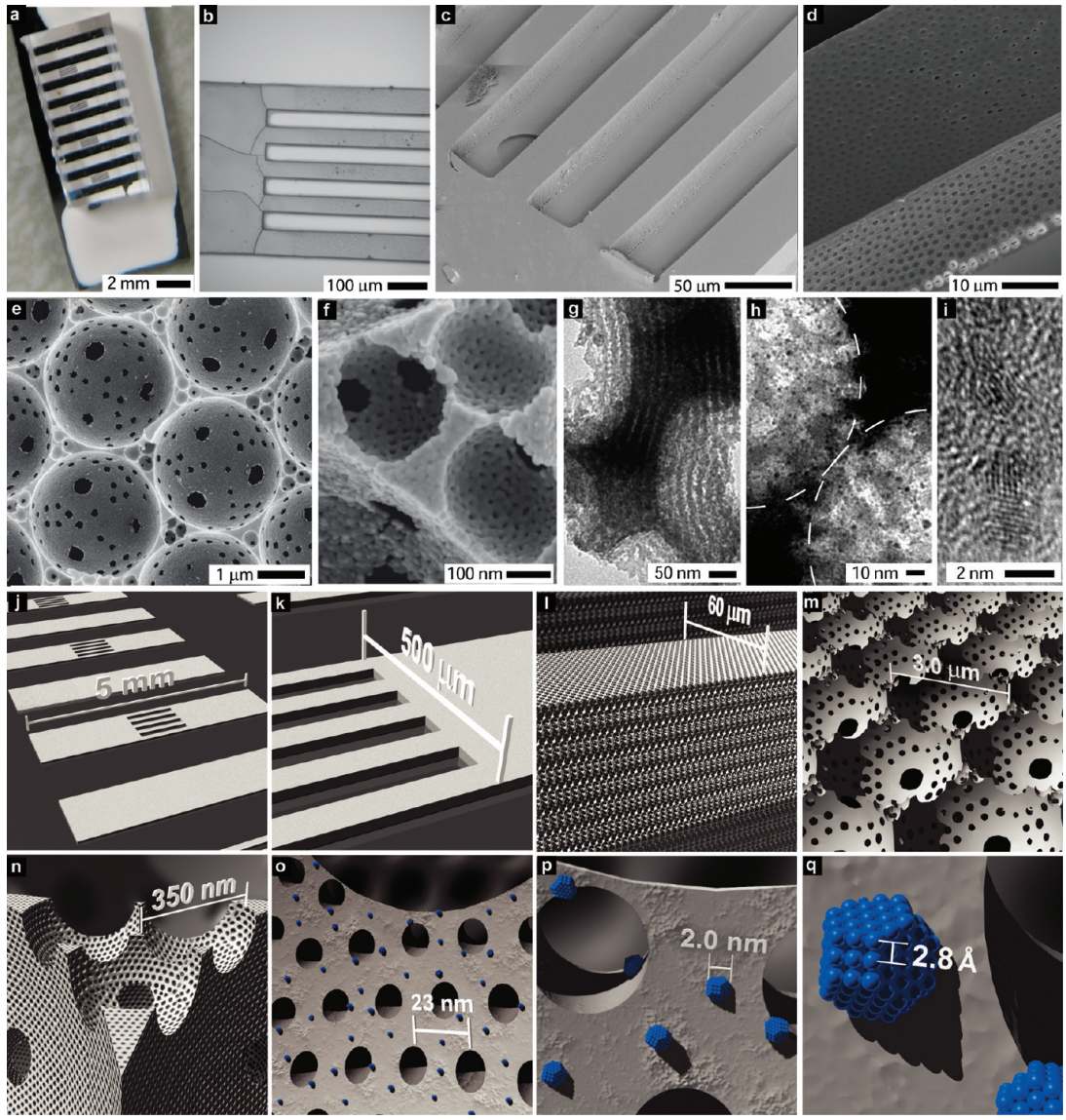

Figure 2. (a) Photograph showing the shape and size of the mold. (b) Light microscope image and (c,d) SEM images of the channel structures. (e) SEM showing channels with a binary colloid-templated structure, consisting of 2.7 and 0.29 μm sized holes. (f) SEM zooming in on the interstitial space of the large colloids revealing that the framework of the porous structure is itself an ordered mesoporous material due to the coassembly of the block copolymer and PUMVS. (g) TEM image of a crushed sample showing the average distance between mesopores of 25 nm. (h) TEM image showing 1−2 nm diameter Pt nanoparticles distributed throughout the material. Dotted lines indicate the colloidal crystal templated structure as a guide. (i) High-resolution TEM resolving Pt lattice fringes. Schematic representation of the eight structural levels in the final material. (j) Level 1: Macroscopic sample dimension. (k,l) Levels 2 and 3: Two different microchannel sizes. (m,n) Levels 4 and 5: Two-component colloidal self-assembly. (o) Level 6: Microphase separation of the coassembled block copolymer and PUMVS. (p) Level 7: Pt nanoparticle size. (q) Level 8: Pt crystal lattice spacing.

After heat treatment under a reducing atmosphere to 1000 °C, higher resolution TEM images reveal Pt nanoparticles homogeneously distributed throughout the walls of the material giving rise to the seventh structural level (Figure 2h, illustration 2p, and Figure 4a,b). While metal compound loading is usually kept low to avoid negative influence of additives on the structure formation,[32] in the present system Pt loadings of 5 wt % in the final material did not disrupt the order (see Figure 3b and Figure 4). Surprisingly, the particle size was found narrowly distributed around 1−2 nm in diameter. This is quite remarkable considering the high temperature treatment. Impregnated systems, even Pt-alumina catalysts that are commonly used, show much larger particle sizes (>50 nm) after heat treatment to only 800 °C.[33] We further examined the material with powder X-ray diffraction (XRD) to determine the crystallinity of the Pt (see Figure 3c,A). The crystallite size as calculated from the Scherrer equation was 1.1 nm. The crystallinity of the particles was confirmed by high-resolution transmission electron microscopy (HRTEM). The typical lattice spacing, measured from images like Figure 2i, was 2.2 Å, which is close to the lattice spacing of 2.26 Å expected for face-centered cubic (fcc) {111} lattice fringes in platinum. The lattice spacings of the Pt crystals (Figure 2q) constitute the eighth and smallest structural level of our materials.

The final materials exhibited very high porosities. For example, values of 87 and 94% void space were obtained for the system described in Figure 2, excluding or including

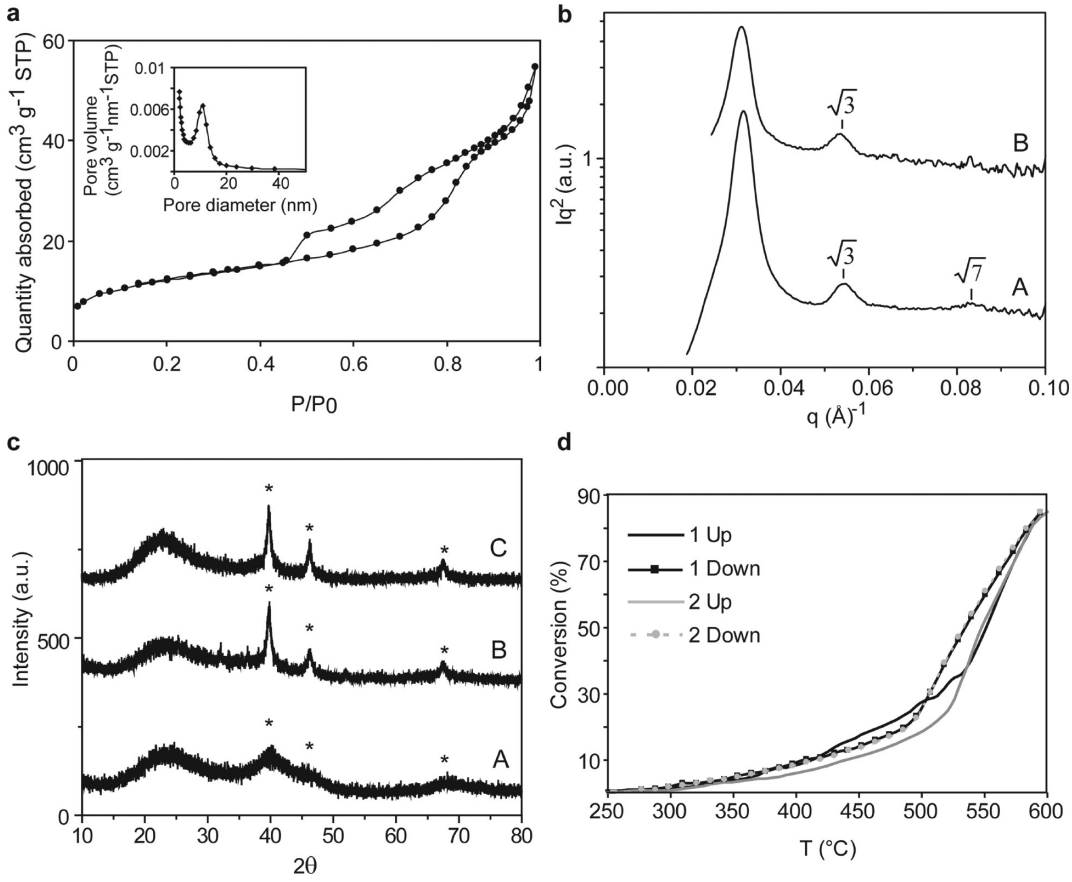

Figure 3. (a) Nitrogen adsorption−desorption isotherm with inset showing corresponding BJH pore size distribution calculated using the adsorption isotherm. (b) SAXS profiles of material heat treated to 1000 °C under an inert atmosphere (A) and after secondary heat treatment to 600 °C in air (B). Tic marks indicate positions of expected reflections for a hexagonal lattice. (c) Powder XRD patterns of (A) material heat treated to 1000 °C showing Pt nanoparticles with domain sizes of 1.1 nm, (B) material post heat treated to 600 °C in air for one minute showing Pt nanoparticles with domain sizes of 10.2 nm and (C) material post heat treated to 600 °C in air for an additional 10 h showing Pt nanoparticles with domain sizes of 11.0 nm. Expected Pt peaks are labeled with asterisks. (d) Methane conversion (activity) as a function of the reaction temperature during two heating/cooling cycles. Conditions: 15 mg of ceramic material; feed gas composition, 1 vol % CH_4, 4 vol % O_2 in balance He, total flow rate 130 mL/min, heating and cooling rate 2.5 °C/min. Other conditions and the experimental procedure are specified in the Supporting Information.

the micromold channels, respectively (see calculation in the Supporting Information). Such high porosities are typically only obtained in foams and aerogels[34] with some exceptions.[35] However, the use of monolithic aerogels and foams is limited to static environments by their low tensile strength, resulting from significant variations in the ratio of wall thickness to pore size and stress concentrations at interparticle necks.[36] In contrast, the walls of the present materials are much more uniform, which may result in superior strength.

The stability of the framework, sintering of the catalyst and catalytic activity of these materials were tested up to 600 °C in an oxidizing environment. Thermogravimetric analysis (TGA) under these conditions revealed that the weight of the pyrolyzed structure did not change substantially (see Supporting Information, Figure S1) exhibiting a loss of less than 5%, which was most likely due to gradual desorption of water below 350 °C, combustion of residual carbon in the material between 350−550 °C, and the formation of a passivating oxide layer at the surface at approximately 575 °C. Postpyrolysis order retention was verified by SAXS. The repeat spacing slightly increased by 0.3 to 20.2 nm, which is within the range of variation between samples (see Figure 3b,B). TGA and SAXS data thus confirm that the material is physically stable under oxidizing conditions up to temperatures at least as high as 600 °C in air. Catalyst sintering was investigated with a combination of TEM and XRD, comparing materials reheated using 5 °C/min ramps and kept at 600 °C in air for 1 min with materials reheated and maintained at 600 °C in air for an additional 10 h. After only 1 min at 600 °C a few larger particles of approximately 10 nm diameter were observed by TEM in addition to the desired 1−2 nm particles (see Figure 4c,d). The average crystallite size (10.2 nm) was determined from the XRD data using the Scherrer equation (see Figure 3c,B). After an additional 10 h at 600 °C, only a slight further increase in the crystallite size to 11.0 nm was calculated from the XRD profile and corroborated with TEM (see Figures 3c,C and 4e). Interestingly, 11 nm is also the size of the mesopores, suggesting that the framework may prevent further particle growth beyond the confines of the mesopores. For the particular case where the Pt particles block the mesopores, a hierarchical pore structure is ideal for its ability to prevent loss of activity by providing multiple access routes to the catalyst.

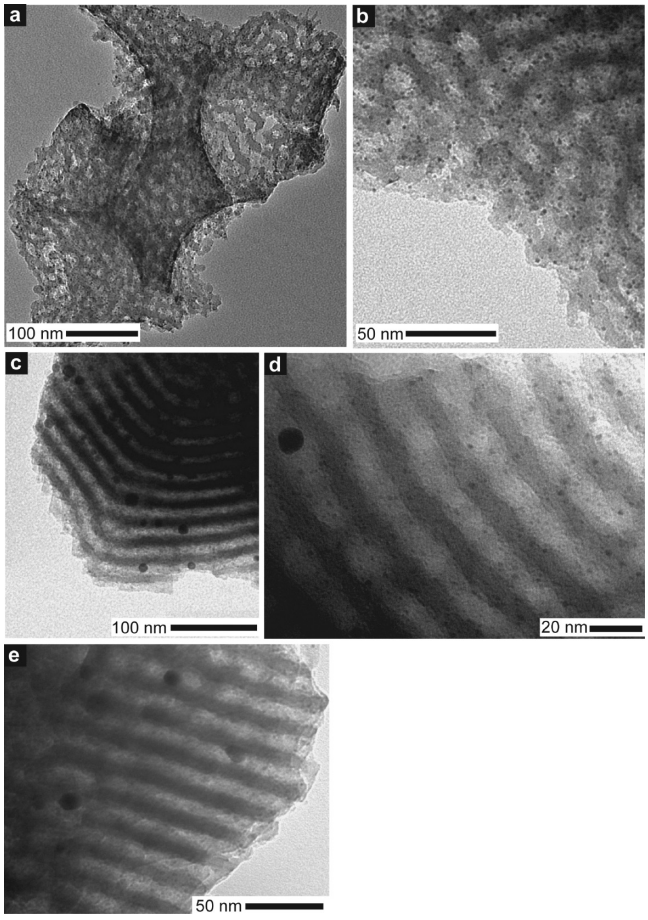

Figure 4. (a,b) TEM images showing the Pt nanoparticles homogeneously distributed throughout the material. (c,d) TEM images of material post heat treated to 600 °C in air for 1 min and (e) for an additional 10 h.

The catalytic activity and thermal stability of the mesoporous ceramics was tested in the total oxidation (combustion) of methane,[37] a reaction relevant to energy technology and environmental catalysis. It should be noted that these experiments were primarily performed as proof-of-principle experiments to demonstrate feasibility of the materials as catalyst supports, as further optimization to obtain high conversions would clearly be necessary, but was beyond the scope of this study. Figure 3d presents the catalytic activity (conversion) as a function of the reaction temperature for two heating−cooling cycles. The methane conversion versus temperature plots show the typical hysteresis behavior observed for platinum-catalyzed methane oxidation during heating and subsequent cooling cycles. The almost identical curves for the cooling cycles suggest that the catalytic activity of the material became stable after the first heating cycle. The strong change of the slope of the conversion versus time curve at approximately 540 °C is probably due to a change of the reaction mechanism induced by the transition from PtOx surface species to metallic Pt upon heating to higher temperatures. The catalytic tests clearly showed the potential of the developed ceramics for catalytic applications at high temperature such as methane oxidation. The system combines excellent size control and high thermal stability of the catalytically active platinum with high structural flexibility rendering this system especially interesting for size-selective catalysis, monolith- and microreactor applications.

Acknowledgment. The authors thank Shahyaan Desai for help with the PDMS mold synthesis, Judy Cha for help with the HRTEM experiments, and Chris Orilall for help with the XRD experiments. Poorna Rajendran and Ian Hosein are acknowledged for discussions on colloidal assembly. The financial support of the National Science Foundation (awards DMR-0605856 and DMR-0404195) are gratefully acknowledged. This work made use of the Soft Matter Cluster and the Integrated Advanced Microscopy facilities of the Cornell Center for Materials Research (CCMR) with support from the National Science Foundation Materials Research Science and Engineering Centers (MRSEC) program (DMR 0520404) and X-ray capability supported by Department of Energy BER Grant DE-FG02-97ER62443.

Supporting Information Available: Experimental section, figure, and porosity calculation. This material is available free of charge via the Internet at http://pubs.acs.org.

References

(1) Baer, E.; Hiltner, A.; Morgan, R. J. *Phys. Today* **1992**, *45*, 60–67.
(2) Yang, P. D.; Deng, T.; Zhao, D. Y.; Feng, P. Y.; Pine, D.; Chmelka, B. F.; Whitesides, G. M.; Stucky, G. D. *Science* **1998**, *282*, 2244–2246.
(3) Yuan, Z. Y.; Su, B. L. *J. Mater. Chem.* **2006**, *16*, 663–677.
(4) Holland, B. T.; Abrams, L.; Stein, A. *J. Am. Chem. Soc.* **1999**, *121*, 4308–4309.
(5) Huang, L. M.; Wang, Z. B.; Sun, J. Y.; Miao, L.; Li, Q. Z.; Yan, Y. S.; Zhao, D. Y. *J. Am. Chem. Soc.* **2000**, *122*, 3530–3531.
(6) Kuang, D. B.; Brezesinski, T.; Smarsly, B. *J. Am. Chem. Soc.* **2004**, *126*, 10534–10535.
(7) Wang, J. J.; Li, Q.; Knoll, W.; Jonas, U. *J. Am. Chem. Soc.* **2006**, *128*, 15606–15607.
(8) Zheng, Z.; Gao, K.; Luo, Y.; Li, D.; Meng, Q.; Wang, Y.; Zhang, D. *J. Am. Chem. Soc.* **2008**, *130*, 9785–9789.
(9) Taguchi, A.; Smatt, J. H.; Linden, M. *Adv. Mater.* **2003**, *15*, 1209–1211.
(10) Chai, G. S.; Shin, I. S.; Yu, J. S. *Adv. Mater.* **2004**, *16*, 2057–2061.
(11) Zhang, F. Q.; Yan, Y.; Yang, H. F.; Meng, Y.; Yu, C. Z.; Tu, B.; Zhao, D. Y. *J. Phys. Chem. B* **2005**, *109*, 8723–8732.
(12) Ryoo, R.; Joo, S. H.; Jun, S. *J. Phys. Chem. B* **1999**, *103*, 7743–7746.
(13) Kamperman, M.; Garcia, C. B. W.; Du, P.; Ow, H. S.; Wiesner, U. *J. Am. Chem. Soc.* **2004**, *126*, 14708–14709.
(14) Sung, I. K.; Christian; Mitchell, M.; Kim, D. P.; Kenis, P. J. A. *Adv. Funct. Mater.* **2005**, *15*, 1336–1342.
(15) Sonnenburg, K.; Adelhelm, P.; Antonietti, M.; Smarsly, B.; Noske, R.; Strauch, P. *Phys. Chem. Chem. Phys.* **2006**, *8*, 3561–3566.
(16) Christian; Mitchell, M.; Kim, D. P.; Kenis, P. J. A. *J. Catal.* **2006**, *241*, 235–242.
(17) Kim, E.; Xia, Y. N.; Whitesides, G. M. *Adv. Mater.* **1996**, *8*, 245–247.
(18) Kitaev, V.; Ozin, G. A. *Adv. Mater.* **2003**, *15*, 75–78.
(19) Malenfant, P. R. L.; Wan, J.; Taylor, S. T.; Manoharan, M. *Nat. Nanotechnol.* **2007**, *2*, 43–46.
(20) Bartlett, P.; Ottewill, R. H.; Pusey, P. N. *Phys. Rev. Lett.* **1992**, *68*, 3801–3804.
(21) Velikov, K. P.; Christova, C. G.; Dullens, R. P. A.; van Blaaderen, A. *Science* **2002**, *296*, 106–109.
(22) Leunissen, M. E.; Christova, C. G.; Hynninen, A. P.; Royall, C. P.; Campbell, A. I.; Imhof, A.; Dijkstra, M.; van Roij, R.; van Blaaderen, A. *Nature* **2005**, *437*, 235–240.
(23) Templin, M.; Franck, A.; DuChesne, A.; Leist, H.; Zhang, Y. M.; Ulrich, R.; Schadler, V.; Wiesner, U. *Science* **1997**, *278*, 1795–1798.
(24) Yajima, S.; Hayashi, J.; Omori, M. *Chem. Lett.* **1975**, 931–934.
(25) Li, Y. L.; Kroke, E.; Riedel, R.; Fasel, C.; Gervais, C.; Babonneau, F. *Appl. Organomet. Chem.* **2001**, *15*, 820–832.

(26) Shah, S. R.; Raj, R. *Acta Mater.* **2002**, *50*, 4093–4103.
(27) Kamperman, M.; Du, P.; Scarlat, R. O.; Herz, E.; Werner-Zwanziger, U.; Graf, R.; Zwanziger, J. W.; Spiess, H. W.; Wiesner, U. *Macromol. Chem. Phys.* **2007**, *208*, 2096–2108.
(28) Hartley, F. R. *Chem. Rev.* **1969**, *69*, 799–844.
(29) Pt can also act as a catalyst for hydrosilation reactions coupling Si−H to C═C in PUMVS.[28]
(30) Barrett, E. P.; Joyner, L. G.; Halenda, P. P. *J. Am. Chem. Soc.* **1951**, *73*, 373–380.
(31) Finnefrock, A. C.; Ulrich, R.; Toombes, G. E. S.; Gruner, S. M.; Wiesner, U. *J. Am. Chem. Soc.* **2003**, *125*, 13084–13093.
(32) Bronstein, L. M. *Top. Curr. Chem.* **2003**, *226*, 55–89.
(33) Osaki, T.; Nagashima, K.; Watari, K.; Tajiri, K. *Catal. Lett.* **2007**, *119*, 134–141.
(34) *Handbook of Chemistry and Physics*; CRC Press [HTML and PDF Electronic annual], 1999.
(35) Schroden, R. C.; Al-Daous, M.; Blanford, C. F.; Stein, A. *Chem. Mater.* **2002**, *14*, 3305–3315.
(36) Woignier, T.; Phalippou, J.; Hdach, H.; Larnac, G.; Pernot, F.; Scherer, G. W. *J. Non-Cryst. Solids* **1992**, *147*, 672–680.
(37) Gelin, P.; Primet, M. *Appl. Catal. B* **2002**, *39*, 1–37.

NL901293P

Supporting Information

Experimental

Block copolymer synthesis: The poly(isoprene-block-dimethylaminoethylmethacrylate) (PI-*b*-PDMAEMA) was polymerized by anionic polymerization as previously reported.[38, 39] Gel permeation chromatography (GPC) was used to determine the molecular weight of the first block (polyisoprene, PI) and the polydispersity of the block copolymer. ^{1}H NMR was used to determine the overall molecular weight of the block copolymer. The resulting polymer had a molecular weight of 31 kg mol^{-1} comprised of 33 wt.-% PDMAEMA with a net polydispersity of 1.04.

Packed beds of PS spheres in PDMS microchannels: To make the PDMS molds a silicon master was photolithographically replicated as described elsewhere.[40] Polystyrene (PS) spheres were purchased from Polysciences and used as received. Best results were obtained using the following procedure: A 2.7 wt % suspension of the 3 μm PS spheres was concentrated to a 15 wt % solution. 350 nm PS spheres (2.7 wt% in water) were added to the 3 μm PS spheres, resulting in a relative concentration ratio of $C_{350nm}/C_{3\mu m}$ of 0.08. The suspension was sonicated for 1 min to ensure complete dispersion of the particles. Silicon substrates were soaked in freshly prepared piranha solution (Concentrated H_2SO_4 and 30 wt % H_2O_2, in a 2:1 v/v mixture) for 30 min, rinsed several times with water, and dried under flowing nitrogen. The PDMS mold was mounted on the freshly cleaned substrate and placed on a hotplate at 30 °C. A drop of PS sphere suspension (20 μl) was placed at one end of the channels and left for several hours to complete the packing process.[17]

These optimized conditions were found by varying the PS sphere sizes, concentrations and assembly temperature. PS sphere sizes tested included combinations of 16.0, 3.0, 2.0 and 1.0 μm diameter spheres with 1.0 μm, 600, 350, 200 and 100 nm sized beads. It was found that very large beads (16 μm) did not flow into the 60 μm channels, small sphere size ratios ($d_{large}/d_{small} < 2$) did not lead to binary lattices and large sphere size ratios ($d_{large}/d_{small} > 30$)

led to poor order. The concentration ratio of the spheres $C_{350nm}/C_{3\mu m}$ was varied between 0.017 and 0.17. A low $C_{350nm}/C_{3\mu m}$ led to inhomogeneous crystal formation, where parts of the crystal were composed of 3 μm spheres only, whereas a high $C_{350nm}/C_{3\mu m}$ led to poor order. The assembly temperature was varied between 0 and 60°C. Assembly temperatures above 40 °C led to water evaporation within the channels, causing bubble formation and poor structure formation. For temperatures between 0 and 40 °C the assembly process proceeded faster for higher temperatures, but no significant changes in the resulting colloidal crystal were observed.

Larger colloidal crystals for physisorption, powder X-ray diffraction (XRD), stability and activity measurements were made by convective assembly. A 1.2 wt% suspension of 3 μm and 350 nm PS spheres with a relative concentration ratio of $C_{350nm}/C_{3\mu m}$ of 0.08 was placed in a vial and sonicated for 1 min to ensure complete dispersion of the particles. The solution was transferred to a glass Petri dish and freshly cleaned substrates were dipped diagonally into the particle solution. The setup was placed in an oven at 60 °C. Samples were left overnight until the liquid evaporated.

Infiltration: The five component infiltration solution consisted of hexane as a solvent, the block copolymer (PI-*b*-PDMAEMA), the ceramic precursor, a radical initiator and the catalyst nanoparticle precursor. The (1,5-cyclooctadiene) dimethylplatinum (Pt-DMCOD) was synthesized as described previously.[41] The anhydrous hexane (Aldrich), the ceramic precursor, Ceraset (KiON Corp.) and the radical initiator, dicumyl peroxide (Aldrich) were used as received. Hexane was chosen as a solvent, because it dissolves all components, but does not dissolve the PS spheres. Other solvents, like THF, toluene and chloroform led to significant deformations of the colloid shape, even when crosslinked PS spheres were used.

In a typical synthesis, 0.10 g of block copolymer was dissolved in 0.6 g anhydrous hexane in a 20 mL vial. 0.20 g of the ceramic precursor was added and the solution was stirred for 1h. Next, 0.0141 g Pt-DMCOD and 0.009 g radical initiator (1 wt.-% with respect

to the mass of PUMVS added) were added and the vial was stirred for another 15 min. A drop of the block copolymer/ precursor solution was subsequently placed at one side of the PDMS mold. Samples were left for several hours until the liquid evaporated followed by crosslinking of the PUMVS at 130 ºC for 3 h. All steps (preparation of the solution, infiltration and crosslinking of the ceramic precursor) were carried out in a glove box under a nitrogen atmosphere owing to the sensitivity of the PUMVS to moisture.[27] The composite was finally heat treated using 1 ºC min^{-1} ramps under argon 95%/hydrogen 5% up to 1000 ºC for conversion into the high-temperature ceramic material and reduction of the catalyst.
Stability tests: Materials were reheated using 5 ºC min^{-1} ramps in air up to 600 ºC.

Structure Characterization

The films were sputtered with gold before being characterized with SEM. SEM images were obtained on a LEO 1550 field-emission scanning electron microscope. For TEM, samples were crushed and then dispersed in ethanol. Bright field TEM micrographs were taken on a Tecnai T12 Spirit Twin TEM/STEM operating at 120 kV and high resolution energy filtered (zero loss) TEM was performed on a Tecnai F20 with a Gatan Tridium Spectrometer at 200 kV. Small Angle X-Ray Scattering (SAXS) data were collected on a Rigaku RU300 copper rotating anode X-ray spectrometer (λ = 1.54 Å) operated at 40 kV and 50 mA. X-rays were monochromated with a Ni filter and focused using orthogonal Franks mirrors. SAXS patterns were collected with a homebuilt 1 K × 1 K pixel CCD detector similar to that described in ref. 42. PXRD was performed on a Scintag XDS 2000, with a scan rate of 0.1° min^{-1}. Thermogravimetric Analysis (TGA) was performed using a Netzsch Jupiter 449 C instrument with a gas flow of 50 mln min^{-1} of 20% O_2 in He. Physisorption was performed on a Micromeritics ASAP 2020 using nitrogen as the adsorption gas.

Catalytic Tests were carried out by mixing 15 mg of the 100 – 200 μm fraction of the catalyst with 70 mg α-Al_2O_3 of 100-200 μm. This mixture was shaken until a homogeneous mixture was obtained, which was subsequently loaded into a quartz U-tube with an inner

diameter of 5 mm. The catalyst bed was fixed by quartz wool plugs. The quartz U-tube was placed in a tubular oven (Carbolite Furnaces) and connected to a mass flow controller (Brooks, 5895E) and gas chromatograph (Hewlett Packard 6890N, equipped with GS GasPro column and capable of automatic gas sampling) by Swagelok couplings with Teflon O-rings. A manometer was used to monitor the pressure before the catalyst bed, which was constant at 0 barg during all experimental conditions.

Each catalytic experiment consisted of two cycles from 200 to 600°C and back with a heating and cooling ramp of 2.5 °C min^{-1}. Prior to each run, the catalyst was pre-treated at 200 °C in the reaction mixture of 1 vol% CH_4, 4 vol% O_2 in balance He. The total flow during each run was 130 mL min^{-1}. The experimental conditions were set so that the conversion never reached 100%. Carbon dioxide was the only reaction product detected. Blanc experiments demonstrated that the diluent, α-Al_2O_3 was not active under the chosen conditions.

TGA analysis

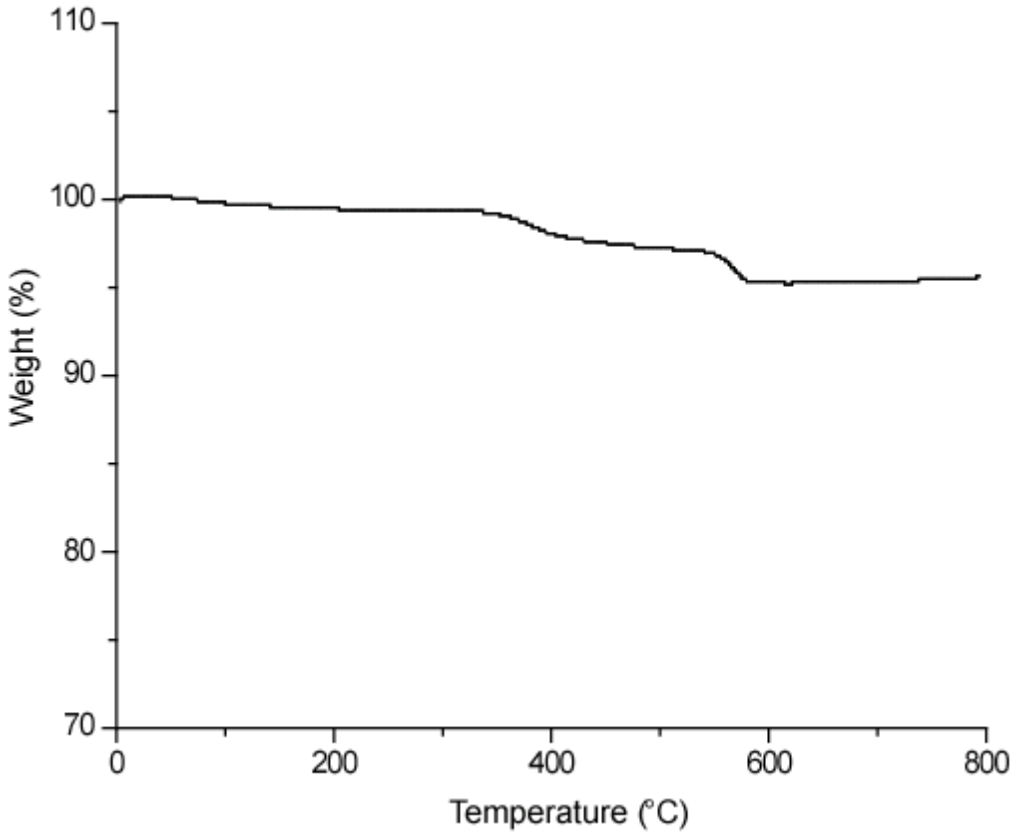

Figure S1: TGA analysis. Ceramic material was heated at 5 °C/min to 850 °C under flowing air.

Porosity

The porosity is calculated assuming the housing around the monolith would fit just around the sample. The 12 small and 6 large air-channels in this volume give rise to a porosity of:

$$\phi_{ch} = \frac{V_{sc} + V_{lc}}{V_{sample}} = \frac{12 \cdot 60 \cdot 950 + 6 \cdot 500 \cdot 5000}{12 \cdot 500 \cdot 5000} = 0.52$$

where ϕ_{ch} is the porosity from the channels, V_{sc} is the volume of the small channels, V_{lc} is the volume of the large channels and V_{sample} is the volume of the entire sample.

The porosity from the colloidal crystal templating is calculated assuming the large spheres pack in a fcc lattice. Calculations and experimental SEM data show that for a sphere size ratio of 350 nm/3.0 μm = 0.117 one tetrahedral site holds 20 small spheres and an

octahedral site 69. There are two tetrahedral sites and one octahedral site for each large sphere. Therefore:

$$\phi_{cc} = \frac{4\left(\frac{4}{3}\pi r_{large}{}^3 + (2\cdot 20 + 69)\frac{4}{3}\pi r_{small}{}^3\right)}{V_{fcc}} = 0.84$$

where ϕ_{cc} is the porosity from the colloidal crystal, V_{fcc} is the volume of one cubic fcc unit cell and r_{large} (1350 nm) and r_{small} (145 nm) the radius of the large and small spheres, respectively. The mesopores in the wall give rise to porosity of the framework. From the lattice parameter determined by SAXS (19.9 nm) together with the BJH average pore size (11 nm) an additional porosity of:

$\phi_m = 0.21$

arises, where ϕ_m is the porosity from the mesoporous framework.

The overall porosity of the material including the micromold channels is therefore:

$$\phi_{total} = \phi_{ch} + (1-\phi_{ch})\phi_{cc} + (1-((1-\phi_{ch})\phi_{cc} + \phi_{ch}))\phi_m = 0.94$$

and the overall porosity of the material excluding the micromold channels is:

$$\phi_{total} = \phi_{cc} + (1-\phi_{cc})\phi_m = 0.87$$

[38] S. Creutz, P. Teyssie, R. Jerome, *Macromolecules* **1997**, *30*, 6.

[39] M. Kamperman, M. Fierke, C. B. W. Garcia, U. Wiesner, *Macromolecules* **2008**, *41*, 8745.

[40] D. C. Duffy, J. C. McDonald, O. J. A. Schueller, G. M. Whitesides, *Analytical Chem.* **1998**, *70*, 4974.

[41] H. C. Clark, L. E. Manzer, *J. Organometal. Chem.* **1973**, *59*, 411.

[42] M. W. Tate, E. F. Eikenberry, S. L. Barna, M. E. Wall, J. L. Lowrance, S. M. Gruner, *J. Appl. Cryst.* **1995**, *28*, 196.